Open Access

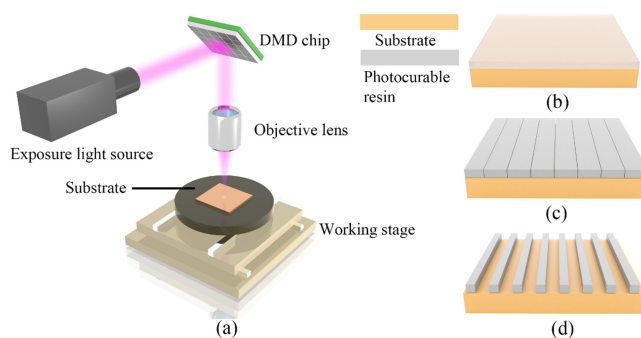# Rapid Prototyping of a Dammann Grating in DMD-Based Maskless Lithography

Qi Zheng
Jinyun Zhou
Qiming Chen
Liang Lei
Kunhua Wen
Yiming Hu

Rapid Prototyping of a Dammann Grating in DMD-Based Maskless Lithography

Qi Zheng [ORCID]**, Jinyun Zhou, Qiming Chen, Liang Lei,
Kunhua Wen** [ORCID]**, and Yiming Hu**

School of Physics and Optoelectronic Engineering, Guangdong University of Technology,
Guangzhou 510006, China

Abstract: Microstructures are fabricated with a fast fabrication speed, submicron-scale precision and a minimum feature size of 1.5 μm. The proposed rapid prototyping fabrication method takes advantage of the maskless lithography technique based on a digital mirror device (DMD) and photocurable resin, which has a broad range of uses in three-dimensional (3D) printing. To illustrate the feasibility of this method, a Dammann grating is fabricated. Using a series of experiments and optimized designs, we analyze the characteristics of the photocurable resin, quantify the dose modulation for lithography and redesign the mask pattern. Consequently, a Dammann grating with a 50% diffraction efficiency is successfully fabricated, which can not only guarantee the precision but also maintain the fabrication speed. This work demonstrates the potential of this method to rapidly and directly manufacture binary optical elements or structures at the nanoscale based on photocurable resin and DMD-based maskless lithography.

Index Terms: Maskless lithography, rapid prototyping, micro-structure, binary optical element, Dammann grating.

1. Introduction

To meet the changing needs associated with the fabrication of optical elements, maskless lithography has been used for the fabrication of micro- and nanoscale structures. At present, several methods are used to fabricate binary optical elements, such as electron-beam (e-beam) lithography [1]–[3], two-photon lithography (2PL) [4]–[6], and scanning-probe-based techniques [7], [8]. However, these maskless lithography methods have complicated processes, long manufacturing times and high cost. There is one maskless lithography method based on a digital mirror device (DMD) that broadly uses fabrication of micro- and nano-structures at present [9]–[13]. A DMD consists of an array of up to two million individually mirrors, which can replace the mask in mask lithography. Compared to conventional mask lithography, this virtual mask can change the image of the layer generated instantaneously. DMD-based maskless lithography is low cost and the image of the whole layer is generated at once, making it a much faster process. With the advancement of DMD-based lithography, a submicron structure has been achieved, showing the potential for nanoscale structures to be constructed using this inexpensive and efficient method.
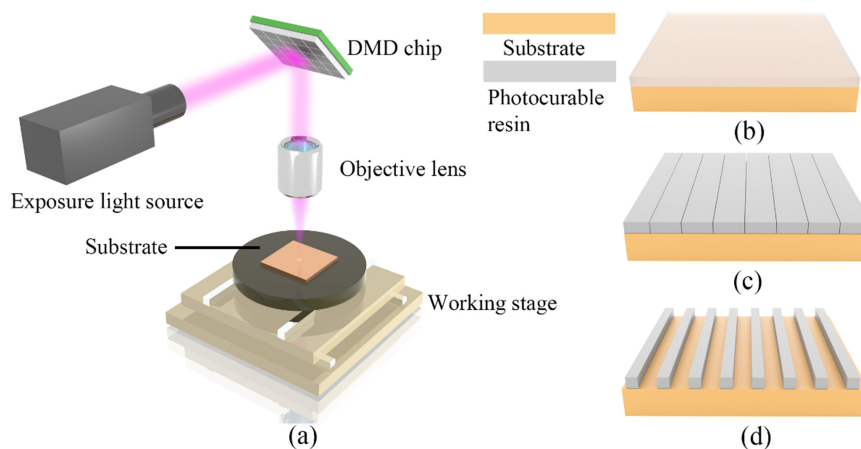
Fig. 1. (a) Schematic view of the digital micromirror device (DMD)-based maskless photolithography system and fabrication process of a grating with a photocurable resin: (b) coat spin, (c) exposure, and (d) development and spin dry to finish the fabrication procedure.

With the advancement in maskless lithography technology and 3D printing, customized aspheric imaging lenses have achieved success [14]. This success demonstrates the potential of this method to rapidly manufacture optical components or systems based on micro-stereolithography and photocurable resin. Photocurable resin has broad applications in the field of 3D printing and fabrication of microstructures [15]–[17]. However, there has been little research focused rapid prototyping of optical element on the microscale.

Here, to achieve a higher efficiency, we report a time- and cost-effective method for the fabrication of optical components using DMD-based lithography and photocurable resin. This procedure includes three steps. The pattern is created and transferred to a CAD file, and the computer converts the mask image into binary data to control the DMDs to generate a virtual mask. Photocurable resin uses DMD-based maskless lithography to generate the structure. The whole process of maskless lithography requires only 10 minutes. First, photocurable resin via spin-coating on a substrate. Then, it is exposed by DMD-based maskless lithography, and the structure is generated after development.

To illustrate the feasibility of the method, a Dammann grating is manufactured rapidly and directly by DMD-based maskless lithography and a photocurable resin. The Dammann grating, originally demonstrated by Dammann and Gortler [18], can create an array of uniform intensity spots in the Fourier transforming plane. Dammann gratings are widely used in the fields of optical communication, optical computing, and image processing [19]–[21]. The Dammann grating is a typical binary optical element whose binary phase structure is easily fabricated by modern lithographic techniques [18]–[23]. However, the structure of the Dammann grating is complex. Because the quality of the structure is related to the optical performance of the Dammann grating, guaranteeing the quality of the structure is significant. Rapid prototyping enables hundreds of experiments to be conducted rapidly, and the experimental data are the basis for improving the quality of the structure. According to the experimental data and an analysis of the characteristics of photocurable resin, we modulate the exposure dose, redesign the mask pattern and improve the fabrication process to improve the performance of the Dammann grating, achieving a diffraction efficiency approaching 50% and a uniformity up to 19.3%.

2. Experimental Setup and Fabrication Procedure

2.1 DMD-Based Maskless Lithography System

A schematic of the DMD-based real-time maskless lithography system is shown in Fig. 1(a). The basic components of the system are the exposure light source, the DMD chip, the objective lens
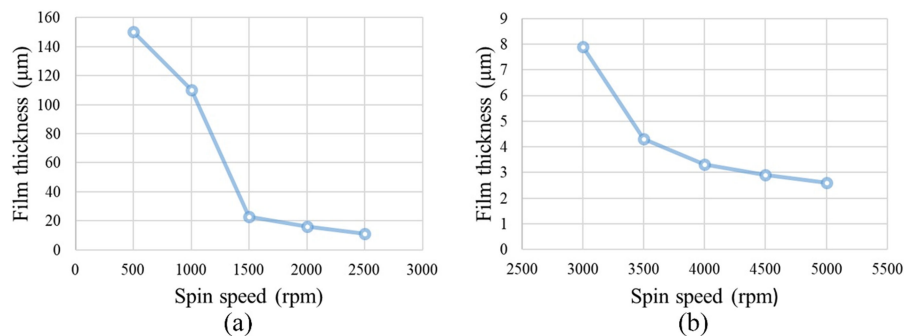
Fig. 2. Photocurable resin spin speed versus thickness. (a) Low speed of spinning and (b) high speed of spinning.

and the working stage. A light-emitting diode (LED) with an output of 5.5 W is used as a near-UV light source with a wavelength of 405 nm. The exposure light source is optimized for high collimation and uniform illumination and then reflected on the DMD chip by a mirror. The DMD chip from Texas Instruments (TI) plays the role of a mask that reflects the near-UV incident light from the light source pixel-by-pixel to generate image frames; the DMD consists of 1560×1024 micromirrors, and each micromirror is $10.8 \times 10.8 \ \mu$m in our system. Every pattern on the DMD chip can be controlled by a computer, which is equivalent to generating a dynamic mask in real time. The computer converts the mask pattern into binary data and controls the DMD to generate corresponding images, replacing traditional physical masks. The uniformity with this maskless lithography is least than 4% and the depth of focus for this technique is 3 μm. The working stage has a travel range of 200 mm $*$ 200 mm in the X-Y plane and 5 mm in the vertical direction with a resolution of 50 nm, which enables us to achieve a large exposure area over the substrate and a precise control of the focus. This lithography technique can generate features on the 2~8 inch substrate and the maximum exposure area is $200 * 200$ mm^2.

Fig. 1(b) shows the fabrication procedure based on DMD-based maskless photolithography with photocurable resin. This procedure consists of three steps: spin-coating, exposure and development. To determine the proper spin-coating conditions, the required information is gathered in experiments, as shown in Fig. 2. The film thickness can be controlled from 2.7 μm to more than 100 μm. In the first step, the viscosity of this photocurable resin (90 cP) is higher than that of traditional photoresist. We need to increase the speed of the spin-coating to achieve the target film thickness. However, when the speed increases up to 5000 rpm, coating defects in the films will become problematic. The depth of the fabricated Dammann grating is limited by the performance of the photocurable resin and the experimental conditions. Otherwise, a thin hydrophobic layer of hexamethyldisilazane (HMDS) can adhere to the substrate and resin to make the substrate hydrophobic to improve the stability of the film and achieve a thinner thickness film [24]. In the second step, the substrate with photocurable resin is exposed to ultraviolet (UV) light with DMD-based maskless lithography, and the power of the ultraviolet light source is 5.5 W. After the UV source illuminates the DMD to expose the substrate, a photochemical reaction is induced, as shown in Fig. 1(c). Next, the substrate is developed in propylene glycol monomethyl ether acetate (PGMEA) for 30 s. Finally, spin drying is employed to remove excess developer on the substrate, and a structure with a sharp surface is fabricated, as shown in Fig. 1(d).

2.2 Design of the Dammann Grating

Many designs and fabrications of Dammann gratings have been introduced in recent decades [23], [25], [26]. In this work, Simulate Anneal Arithmetic (SAA) is applied in this design process, which has been widely used in the design of Dammann gratings [27]–[29]. SAA can find the global optimum of an objective function by a random search, has a strong local search ability and avoids falling into

TABLE 1
Result of Design with SAA

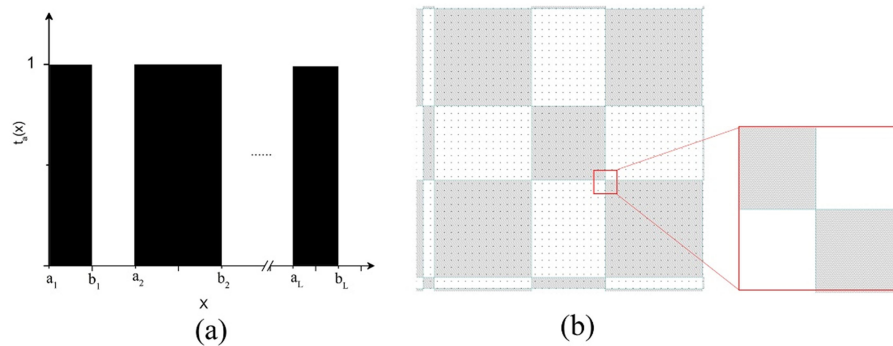| Orders	Jump points coordinate		Total efficiency
5	$a_1 = 0$	$b_1 = 0.0385751$	77%
	$a_2 = 0.3869454$	$b_2 = 0.6516349$	

Fig. 3. (a) Distribution of the piecewise constant transmittance of a one-dimensional DG and (b) the mask pattern of a two-dimensional DG in one period.

a local optimal solution. Finally, four mutation coordinates are attained, and the results are shown in Table 1. The calculation results are in one-dimensional in terms of direction, and the operation of the orthogonal direction can extend to two-dimensional spaces. Next, the designed mask pattern was drawn in L-Edit, which is software for integrated circuit layout design developed by Tanner Research. A schematic of the Dammann grating mask pattern is shown in Fig. 3(b). The device is designed to operate at a wavelength of approximately 850 nm. Thus, the depth for achieving a 2π phase modulation is $h = \lambda/(n_s - 1) \approx 1.7\ \mu m$, where $n_s = 1.51$ is the refractive index of the resin.

2.3 Experimental Exploration and Improvement

Photocurable resin is widely used by 3D printing. Catering for mass production and a wide variety of applications, the photocurable resin we use (Wanhao 3D Printing resin, Wanhao corporation) is very inexpensive and environmentally friendly. However, in terms of microstructure fabrication, the quality of the structures is limited by the resolution limit and curing shrinkage. Based on hundreds of experiments, an optimization of the design and fabrication process is proposed to improve the quality of the structure and the performance of the optics.

It is significant to analyze the dose modulation for building the required microstructures on the photocurable resin. Only the relationship between the exposure dose and the exposure height are quantified, and we can fabricate the appropriate structure. Therefore, we can achieve the designed height of the Dammann grating by modulating the exposure dose. The height of the Dammann grating relates to the diffraction efficiency, because the Dammann grating is a kind of transmission-type phase grating. Thus, we measure the effect of the dose modulation before the fabrication process.

For this photocurable resin, the exposure threshold, Eth, is defined as the minimum exposure dose required for the initial reaction of the resin. Increasing this exposure dose, the height of the
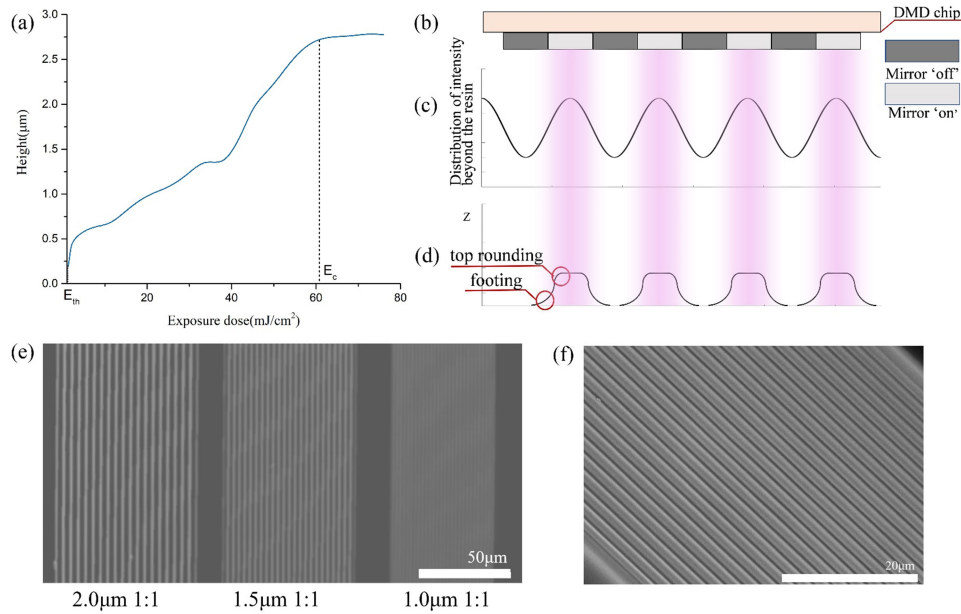
Fig. 4. (a) Measurement of the contrast curve. (b) Mirrors of the DMD chip. (c) Distribution of the intensity. (d) Profiles of the structure. (e) To quantify the resolution limit in this method, a line array was fabricated under the same illumination conditions. (f) SEM image of a 1.5 μm line array.

structure increases until it reaches another exposure threshold, E_c, and E_c is defined as the required exposure dose for the maximum curing height. There value of contrast γ between the exposure dose and the height of resin [30] is shown below:

$$\gamma = \frac{1}{\ln E_c - \ln E_{th}} = \frac{H/H_{total}}{\ln E_c - \ln E_{th}} \qquad (1)$$

where $0 \leq H \leq H_{total}$, $E_{th} \leq E \leq E_c$

In this equation, H and H_{total} represent the exposure height and the maximum thickness of the resin, respectively. The following equation can be derived from (1):

$$E = \exp\left(\frac{\gamma \times H_{total}}{H}\right) + E_{th} \qquad (2)$$

Several 1 mm * 10 mm rectangles with different exposure doses are exposed to the resin with a speed of 5000 rpm. After development, confocal laser scanning microscopy (CLSM, Olympus OLS4100) is used to measure the height of the structure for different exposure doses. Based on these experiments, the experimental data are processed. The contrast curves are obtained as shown in Fig. 4(a).

The resin used in this fabrication process is photocurable resin, which can be identified from the relationship between the exposure dose and height, where the exposure threshold Eth and the contrast γ of the photoresist are 1.2 mJ/cm^2 and 0.2598, respectively, the maximum height of the development, H_{total}, is 2.8 μm, and the required exposure dose is 61 mJ/cm^2. Then, the exposure dose for the structure height can be calculated according to (1) and (2).

We can not only acquire the appropriate exposure dose but also indicate the performance of the photocurable resin from the contrast curve directly. In the region of a low-exposure dose, the contrast curve shows the sensitivity of the photocurable resin for the flare. As shown in Figs. 4(b) and (c), at the edge of the 'on' mirror, there is a clear reduction in the exposure intensity. The flare, which impacts the sidewall of the structure, exists at the edge of the 'off' area and the 'on' area. After the threshold of the initial reaction, Eth, there is an increased structural height with increasing exposure
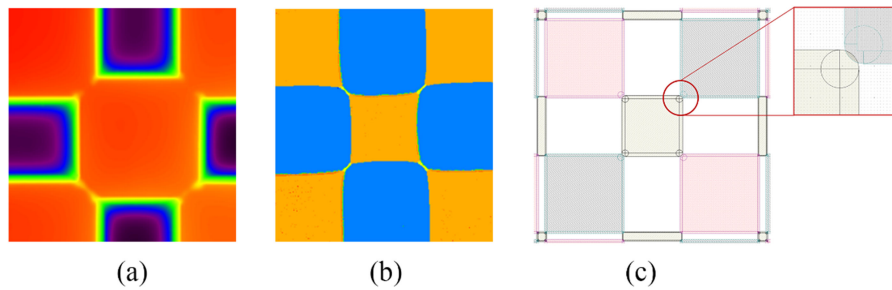
Fig. 5. (a) The corner disappears. (b) The distance between 2 corners is too long and a joining line appears. (c) The mask pattern with two layers after the optimization.

dose. In Fig. 4(d), the flare with a low dose generates the footing of the structure in the 'off' area. With increasing exposure dose, there is a linear region. Then, in the area of a high-exposure dose, the contrast curve is nonlinear and generates the top rounding of the structure. The ideal sidewall is vertical without a top rounding and footing. However, in an actual experiment, the performance of the photocurable resin also affect the footing and top rounding. A higher contrast γ can achieve a weaker effect of the footing, a smaller top rounding and a steeper sidewall. In conclusion, we can deduce the performance of the photocurable resin according to the contrast curve. In addition, the performance of the resin and the resolution limit of lithography are critical to the limitation of the resolution in this method.

The Dammann grating is a composite structure that consists of many individual structures. The minimum structure is a 3.9 μm × 3.9 μm cuboid with a 1.7 μm height. The size is near the resolution limitation. The minimum gap between two individual structures is as short as possible. For example, in Fig. 3(b), the gap between two corners almost disappears. When the size of the gap is smaller than the minimum resolution, the individual structure may combine, and the gap may disappear. The length of the gap depends on the achievable resolution limit. It is essential to quantify the resolution limit to ensure the minimum size of the gap and the structure. To quantify the resolution limit in this method, we fabricate a line array with different widths under the same illumination conditions. As shown in the CLSM image in Fig. 4(e), the array of the 2.0 μm width line and 1.5 μm width line is shown clearly, but the 1.0 μm width lines are not achievable in an actual experiment. In Fig. 5(f), a scanning electron microscopy (SEM, Hitachi S3400N) image shows that the line array with a 1.5 μm width and the gap between the lines is smaller than 1.5 μm. This indicates that the lines of the array intend to merge together with the decreasing width of line. In conclusion, the result indicates that the resolution limit is near 1.5 μm. Therefore, the gap between the two corners should theoretically be 1.5 μm.

For a large exposure area, the flare on the edge of the adjacent images will superimpose, which will increase the density of the flare on the edge. This will decrease the contrast of the structure and occur over the size of the structure. Consequently, individual structures adhere together, as shown in the CLSM image of CLSM Fig. 5(a). Then, when the dose of exposure is too low, the size will decrease, as shown in the CLSM image of Fig. 5(b). In addition, the flare in the corner of square shape generates the joining line between two corners, as shown in Fig. 5(b). Hence, to decrease the flare, the mask pattern is divided into three layers, as shown in Fig. 5(c). The first layer, represented by the light shape, was exposed first. Then, the second layer shown in gray was exposed. The overlapping of the spare flare at two corners can be avoided, which will produce a joining line connecting two corners. The last layer is that shown by the red shapes, which can decrease the spare flare in the gap between two large square shapes. Moreover, we redesigned the shape of the corners to avoid generating unnecessary a joining line, as shown in Fig. 5(c). Sharp corners generate the joining line easily, but a round corner can produce a shorter distance between two corners without a joining line. Then, we designed a series of round corners with different corner

radii. We fabricated and measured the corners in order to select an appropriate corner such that the distance between two corners was near the resolution limit without a joining line.

Moreover, because of the assembly of the molecules and the decrease in the intermolecular distances, photocurable resin will shrink after exposure. The curving shrinkage, a natural characteristic of photocurable resin, is a quantitative expression of the shrinkage in an experiment. In this work, the experimental shrinkage is 3.3%. The size of the designed large square shape is 34.83 μm, and the curving shrinkage can lead to a decrease in the size of the shape of approximately 1 μm. To diminish this effect, we enlarged the exposure area to offset the impact of the curving shrinkage by redesigning the mask pattern. Then, we fabricated and measured the structures to select the appropriate mask pattern.

Fortunately, with rapid prototyping, we were able to design different mask patterns in L-edit software, fabricate the structures and measured their properties within an hour. The fast fabrication procedure and flexibility of DMD-based maskless lithography are advantages of rapid prototyping that enable the fabrication of hundreds of different samples in a short time. This not only accelerates the process of research but also assists in improving the performance of optics based on extensive experimental data. With a continuous improvement in the design and fabrication, the diffraction efficiency of the Dammann grating and the uniformity of the light spot array have been improved. Later, continued improvements led to a doubling of the efficiency to 50%, and the uniformity reached 19%. Next, the results after the improvement are shown in detail.

3. Results

The resin was spin-coated on a glass substrate at 5000 rpm. Then, the thickness of the resin film was approximately 1.8 μm. Next, the mask pattern was exposed on the surface of the resin. After development in PGMEA for approximately 30 s and dry spinning, the surface of the Dammann grating was obtained as shown in Fig. 6(a). CLSM was used to measure the profile of the Dammann grating, as shown in Fig. 6(b) and Fig. 6(c). The measured width of the large square is 35.06 μm, and the designed width is 34.83 μm. Therefore, the deviation is approximately 230 nm (0.66%), which means that the error between the real profile and the design profile has been reduced effectively. Fig. 6(d) shows the sidewall of the structure. The decreasing process of the edge is approximately 1 μm. The top rounding and footing, which are related to the performance and sensitivity of photocurable resin, impact the contrast of the edge. Similarly, it also seriously impacts the gap between two corners. Fig. 6(e) shows the details of the corners and the obtained gap. In Fig. 6(f), the profile of the gap shows that the distance is approximately 1.5 μm, and the top rounding and footing of the corners lead to a high edge contrast.

To estimate the optical performance of the Dammann grating, imaging experiments were carried out, as shown in Fig. 7(a). In the imaging experiment, a laser beam at a wavelength of 850 nm was introduced to illuminate the Dammann grating. In Fig. 7(b), a 5 $\times$ 5 light spot array with uniform intensity was captured by a charge-coupled device (CCD) placed behind the Fourier lens. Fig. 7(c) presents an image of the light spots and the intensity distribution. Fig. 7(d) shows an image of the normalized intensity of a single typical spot. The full width at half maximum (FWHM) for this light spot is approximately 22.5 μm.

According to the intensity distribution of light spot array, the intensity of each spot was shown clearly. The intensity of the light spot with maximum intensity is I_{max} and the intensity of the light spot with minimum intensity is I_{min}. The uniformity of light spots array was defined as:

$$u = \frac{I_{max} - I_{min}}{I_{max} + I_{min}} \tag{3}$$

7 Then, the uniformity u can reach 19.3% and the diffraction efficiency of our grating can reach 50.33%. But, as shown in Fig. 8(a), the high speed of the spin-coating lead to coating defects thus non-uniform resin film generated. In Fig. 8(b), it cannot generate the integrate structure on the rough surface. Therefore, adequately mixing the constituents in the resin before spin-coating is key to maintaining the stability of the resin. However, sometimes this is difficult to control, which
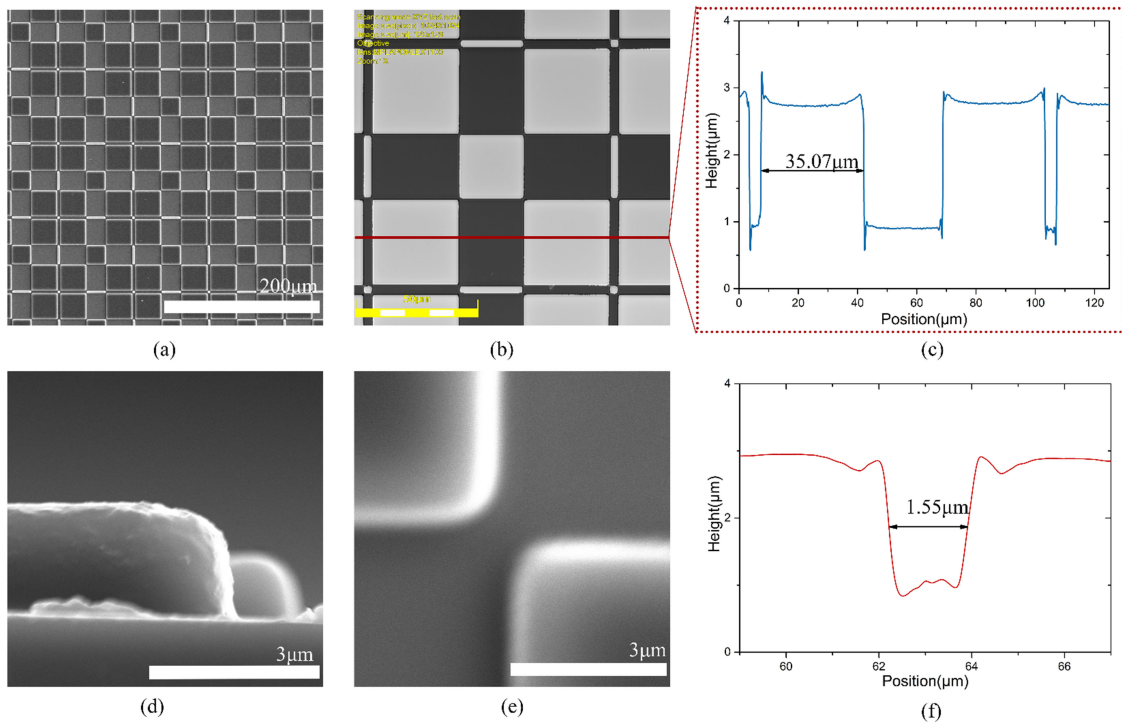
Fig. 6. (a) SEM image of the Dammann grating. (b) CLSM image of the Dammann grating and (c) the profile of the big squares. (d) The sidewall of the resultant structure. (e) SEM image and (f) profile of the gap measured by CLSM.
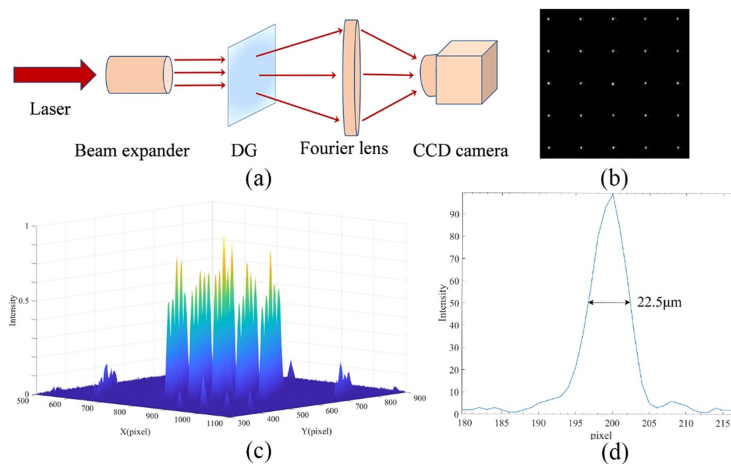

Fig. 7. (a) Schematic diagram of the Dammann grating experimental setup. (b) Normalized intensity distribution of the light spot array. (c) The image of the light spot array. (d) An image of the intensity of a single spot.

impacts the shape of the structure and performance of the optics. The total area of the fabricated Dammann grating is 1 cm * 1 cm. This large-area grating always includes many defects, so the diffraction efficiency and the uniformity of the light spot array are reduced. However, if the speed of the spin-coating is reduced, the film will be thicker, and the structure will not achieve better.
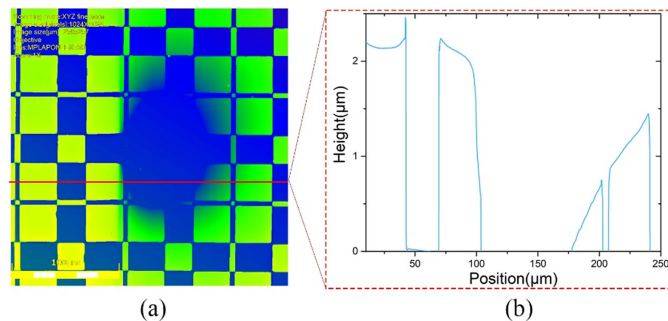
(a)   (b)

Fig. 8. (a) CLMS image of coating defect. (b) Profile of unintegrated structure.

Therefore, enhancing the stability of the photocurable resin is important for the quality of the microscale structure.

4. Conclusions

In this work, we report a time- and cost-effective method for fabricating a Dammann grating using DMD-based maskless lithography and photocurable resin. This rapid prototyping method can directly manufacture the microstructure. The procedure only consists of three steps: spin-coating, exposure and development. It is significant to guarantee the quality of the structure so that the optical performance of the Dammann grating will be reliable. To improve the quality of the structure and the performance of the optics, we quantified the dose modulation in fabricating the required microstructures on the photocurable resin and analyzed the resolution limit to ensure that the minimum gap size and the appropriate structures were obtained. In addition, we optimized the design of the mask pattern to decrease the intensity of the superimposed flare on the edge of the image and the effect of the curving shrinkage of the photocurable resin. We demonstrated the capability of rapidly prototyping optical elements with submicron-scale precision and a minimum feature size of 1.5 μm, which offers a highly reliable solution for rapid prototyping of micro-optics from an optimized design. In addition, with continuous improvements in the design and fabrication, the diffraction efficiency of the Dammann grating and the uniformity of the light spot array were also improved. The diffraction efficiency of the grating could reach 50.33%, the uniformity was better than 20%, and the FWHM of this light spot was approximately 22.5 μm. In conclusion, this work demonstrated the unprecedented potential of photocurable resin and DMD-based maskless lithography for optical fabrication, which will further lead to many novel structures with a tremendous impact on the fabrication of nanostructure and binary optical elements.

Acknowledgment

References

[1] C. Vieu *et al.*, "Electron beam lithography: Resolution limits and applications," *Appl. Surf. Sci.*, vol. 164, no. 1, pp. 111–117, 2000.

[2] M. Drost *et al.*, "Surface-anchored metal–organic frameworks as versatile resists for gas-assisted e-beam lithography: Fabrication of sub-10 nanometer structures," *ACS Nano*, vol. 12, no. 4, pp. 3825–3835, 2018.

[3] N. Jiang *et al.*, "Atom-by-atom fabrication by electron beam via induced phase transformations," *MRS Bull.*, vol. 42, no. 9, pp. 653–659, 2017.

[4] J. K. Gansel *et al.*, "Gold helix photonic metamaterial as broadband circular polarizer," *Science*, vol. 325, no. 5947, pp. 1513–1515, 2009.

[5] K.-S. Lee, R. H. Kim, D.-Y. Yang, and S. H. Park, "Advances in 3D nano/microfabrication using two-photon initiated polymerization," *Prog. Polym. Sci.*, vol. 33, no. 6, pp. 631–681, 2008.

[6] D. Schwärzle, X. Hou, O. Prucker, and J. Rühe, "Polymer microstructures through two-photon crosslinking," *Adv. Mater.*, vol. 29, no. 39, 2017, Art. no. 1703469.

[7] E. U. Haq *et al.*, "Parallel scanning near-field photolithography: The snomipede," *Nano Lett.*, vol. 10, no. 11, pp. 4375–4380, 2010.

[8] F. Huo *et al.*, "Beam pen lithography," *Nature Nanotechnol.*, vol. 5, pp. 637–640, 2010.

[9] X. Ma *et al.*, "Experimental study of numerical optimization for 3-D microstructuring using DMD-based grayscale lithography," *J. Microelectromech. Syst.*, vol. 24, no. 6, pp. 1856–1867, 2015.

[10] B. Yang, J. Zhou, Q. Chen, L. Lei, and K. Wen, "Fabrication of hexagonal compound eye microlens array using DMD-based lithography with dose modulation," *Opt. Exp.*, vol. 26, no. 22, pp. 28927–28937, 2018.

[11] E. J. Mott *et al.*, "Digital micromirror device (DMD)-based 3D printing of poly(propylene fumarate) scaffolds," *Mater. Sci. Eng., C*, vol. 61, pp. 301–311, 2016.

[12] J. Yoon, K. Kim, and W. Park, "Modulated grayscale UV pattern for uniform photopolymerization based on a digital micromirror device system," *Appl. Phys. Lett.*, vol. 111, no. 3, 2017, Art. no. 033505.

[13] L. Huang *et al.*, "Ultrafast digital printing toward 4D shape changing materials," *Adv. Mater.*, vol. 29, no. 7, 2017, Art. no. 1605390.

[14] X. Chen *et al.*, "High-speed 3D printing of millimeter-size customized aspheric imaging lenses with sub 7 nm surface roughness," *Adv. Mater.*, vol. 30, no. 18, 2018, Art. no. 1705683.

[15] N. Sakai, "Photo-curable resin for UV-nanoimprint technology," *J. Photopolym. Sci. Technol.*, vol. 22, no. 2, pp. 133–145, 2009.

[16] T. Nakamura and M. Nakagawa, "Print and imprint method for nanoimprint lithography with high-viscosity photo-curable resins," in *Proc. Int. Conf. Electron. Packag.*, 2017, pp. 443–446.

[17] V. S. D. Voet *et al.*, "Biobased acrylate photocurable resin formulation for stereolithography 3D printing," *ACS Omega*, vol. 3, no. 2, pp. 1403–1408, 2018.

[18] H. Dammann and K. Görtler, "High-efficiency in-line multiple imaging by means of multiple phase holograms," *Opt. Commun.*, vol. 3, no. 5, pp. 312–315, 1971.

[19] C. Zhao, F. Fan, A. Tam, M. Schadt, V. Chigrinov, and H.-S. Kwok, "P-147: Diffractive optical elements based on rewritable photoalignment for transparent display and smart windows," *SID Symp. Dig. Tech. Papers*, vol. 49, no. 1, pp. 1718–1720, 2018.

[20] J. Wang, C. Zhou, W. Jia, Y. Xie, D. Zhao, and C. Xiang, "Direct laser writing lithography technology based on rotating two-dimensional Dammann grating," in *Proc. Holography, Diffractive Optics, Appl.*, vol. 10818, p. 15, 2018.

[21] Y. Xu, X. Han, G. Li, J. Liu, K. Xia, and J. Li, "Vortex and LG01-mode Nd:YAG laser involving a circular Dammann grating," *Opt. Eng.*, vol. 55, no. 5, pp. 1–5, 2016.

[22] H. Dammann and E. Klotz, "Coherent optical generation and inspection of two-dimensional periodic structures," *Optica Acta, Int. J. Opt.*, vol. 24, no. 4, pp. 505–515, 1977.

[23] S. Zhao and P. S. Chung, "Design of a circular Dammann grating," *Opt. Lett.*, vol. 31, no. 16, pp. 2387–2389, 2006.

[24] M. L. Hair and W. Hertl, "Reaction of hexamethyldisilazane with silica," *J. Phys. Chem.*, vol. 75, no. 14, pp. 2181–2185, 1971.

[25] B. Wu, J. Kang, and W. Han, "Design of Dammann grating based on the parallel recombination simulated annealing algorithm," *Optik Int. J. Light Electron Opt.*, vol. 124, no. 17, pp. 2928–2931, 2013.

[26] J. Wang, C. Zhou, J. Ma, Y. Zong, and W. Jia, "Highly efficient reflective Dammann grating with a triangular structure," *Appl. Opt.*, vol. 55, no. 19, pp. 5203–5207, 2016.

[27] J. Turunen, A. Vasara, J. Westerholm, G. Jin, and A. Salin, "Optimisation and fabrication of grating beamsplitters," *J. Phys. D, Appl. Phys.*, vol. 21, no. 10S, pp. S102–S105, 1988.

[28] J. N. Mait, "Design of binary-phase and multiphase Fourier gratings for array generation," *J. Opt. Soc. Amer. A*, vol. 7, no. 8, pp. 1514–1528, 1990.

[29] J. Turunen, A. Vasara, J. Westerholm, and A. Salin, "Stripe-geometry two-dimensional Dammann gratings," *Opt. Commun.*, vol. 74, no. 3, pp. 245–252, 1989.

[30] K. Suzuki and B. W. Smith, *Microlithography: Science and Technology*. New York, NY, USA: Marcel Dekker, 2007.